Review Article

Access this article online

Quick Response Code:

Website: http://www.braincirculation.org

DOI: 10.4103/2394-8108.178544

Magnetic resonance imaging of cerebral blood flow in animal stroke models

Qiang Shen[1,2,3], Timothy Q Duong[1,2,3,4]

Abstract:

Perfusion could provide useful information on the metabolic status and functional status of tissues and organs. This review summarizes the most commonly used perfusion measurement methods: Dynamic susceptibility contrast (DSC) and arterial spin labeling (ASL) and their applications in experimental stroke. Some new developments of cerebral blood flow (CBF) techniques in animal models are also discussed.

Key words:

Arterial spin labeling (ASL), dynamic susceptibility contrast (DSC), functional MRI (fMRI), perfusion MRI

Introduction

Cerebral blood flow (CBF) (tissue perfusion) is tightly regulated, as it is important for adequately delivering oxygen and nutrients to tissues and carrying out waste products. Perfusion could thus provide useful information on the metabolic status and functional status of tissues and organs. For this reason, much effort has been put into its measurement. There exist two main magnetic resonance imaging (MRI) perfusion methods: bolus tracking of an exogenous endovascular tracer and arterial spin labeling (ASL).[1] In this review, the theories of these two methods are briefly discussed and their applications in experimental stroke are summarized. Some new CBF technical developments, including background suppression, high spatial resolution CBF, and ASL-MRI in mice are also discussed. This review mainly discusses works done by our research group.

Perfusion Magnetic Resonance Imaging Methods

The contrast agents commonly used in MRI are based on gadolinium (or Gd^{+3} to be precise), a strongly paramagnetic but toxic substance. It is concealed by an organic complex or compound, which determines the behavior of the contrast agent within the body (e.g., half-life in the body). The paramagnetic effect of gadolinium influences the local magnetic field and leads to a large reduction in the T1 relaxation time and a smaller reduction of T2 relaxation time. A strong reduction can be seen in T2* relaxation time measurements, which probe local magnetic field changes. Injecting such a gadolinium-based contrast agent into the body will lead to local changes in relaxation time depending on the local concentration of the contrast agent. Brain perfusion imaging performed after the intravenous administration of a gadolinium-based contrast agent is referred to as dynamic susceptibility contrast (DSC). DSC utilizes the T_2* effect of a bolus of gadolinium — the fundamental observation is that the agent causes a transient decrease in signal intensity during initial transit through the vasculature.[2,3] DSC is the most commonly used perfusion measurement method in the clinics because of its short acquisition time. By kinetic modeling of the DSC data captured using rapid imaging (most commonly echo planar imaging), CBF, cerebral blood volume (CBV), and mean transit time (MTT) can be derived. The quantification of perfusion information from DSC involves the determination of arterial input function (AIF) and deconvolution operations.[4] In case the blood–brain barrier (BBB) is not intact, the tracer could leak into the extravascular space. In this condition, the contrast agent affects T_1 and T_2* on the tissue compartment,[5] confounding CBF calculation. More sophisticated models of the first pass kinetics are needed to correctly extract

[1]Research Imaging Institute, [2]Departments of Ophthalmology and [3]Radiology, University of Texas Health Science Center, [4]Department of Veterans Affairs, South Texas Veterans Health Care System, San Antonio, Texas, USA

Address for correspondence:
Dr. Qiang Shen, Research Imaging Institute, University of Texas Health Science Center, 8403 Floyd Curl Dr, San Antonio - 78229, Texas, USA.
E-mail: shenq3@uthscsa.edu

Submission: 08-10-2015
Revised: 08-01-2016
Accepted: 12-01-2016

How to cite this article: Shen Q, Duong TQ. Magnetic resonance imaging of cerebral blood flow in animal stroke models. Brain Circ 2016;2:20-7.

CBF and other hemodynamic parameters if BBB integrity is compromised.[6]

By contrast, ASL is a perfusion MRI method for quantitatively measuring cerebral perfusion by taking advantage of using the magnetically labeled blood itself as an endogenous tracer. ASL gives absolute values of perfusion of the tissue by blood. This technique utilizes arterial water as an endogenous diffusible tracer, which is usually achieved by magnetically labeling the incoming blood.[7] Thus, ASL is completely noninvasive, requiring no exogenous contrast agent or ionizing radiation. Repeated measurements can be made, which can be used for dynamic studies [i.e., functional MRI (fMRI)], averaging to enhance signal-to-noise ratio (SNR) and/or to enhance spatial resolution. ASL requires the subtraction of two images, one in which the incoming blood has been labeled and the other in which no labeling has occurred. The typical signal difference, which can be measured in ASL is very small, with the measured ASL signal being approximately 1-1.5% of the tissue signal in the human brain. Thus, in conventional ASL experiments, several repetitions of control and label phases have to be performed to yield sufficient SNR. Efficient background suppression (BS) and image readout strategies exist[8] to overcome these burdens. Original ASL techniques such as continuous[7,9] and pulsed ASL[10,11] tag the blood in larger vessels outside the imaging volume while the newer velocity-selective ASL approach[12] allows tagging blood closer to (and even within) the site of imaging by only labeling spins moving within a certain velocity range independent of location.

Applications of Arterial Spin Labeling and Dynamic Susceptibility Contrast in Animal Stroke Model

Continuous arterial spin labeling (cASL) technique has been widely used in animal stroke studies. Shen *et al*. used cASL technique to measure the acute CBF changes after middle cerebral artery occlusion (MCAO) in permanent[13] and transient MCAO stroke rats.[14,15] Perfusion-diffusion mismatch (perfusion deficit area is larger than diffusion abnormal area) was found presented up to 3 h after occlusion [Figure 1]. A CBF viability threshold yielding the lesion volumes (LV) at 3 h that best approximated the 2,3,5-triphenyltetrazolium chloride (TTC) infarct volumes at 24 h was found to be 0.30 ± 0.09 mL/g/min (57% ± 11% reduction). Automated cluster analysis of the perfusion and diffusion data was also been used to objectively cluster pixels of different tissue fates. Shen *et al*. developed and applied an improved algorithm based on the automated ISODATA (self-organizing data analysis algorithm) technique to characterize the spatiotemporal dynamic evolution of ischemic brain injury based on high-resolution quantitative perfusion and diffusion measurements.[16] The automated

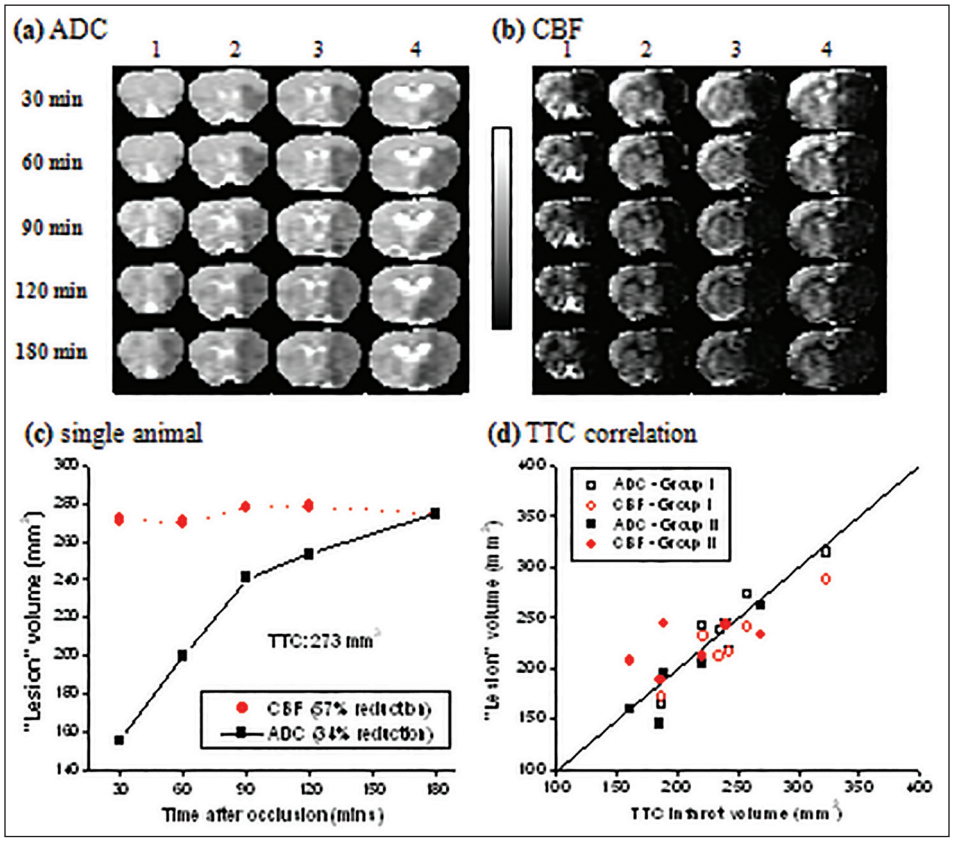

Figure 1: *Representative (a) ADC and (b) CBF maps from one animal. The gray scale bar indicates ADC ranges from 0 mm²/s to 0.001 mm²/s and CBF ranges from -1 mL/g/min to 2 mL/g/min (c) Temporal progression of ADC-defined and CBF-defined lesion volumes (LVs) determined by using the group average viability thresholds (57% and 30% reduction for CBF and ADC, respectively) (d) Correlation ADC-defined or CBF-defined LV versus TTC-infarct volumes. Correlation coefficient (r) and one-to-one correspondence (y = x) coefficient (R) were calculated. Group I CBF (r = 0.98, R = 0.95), group II CBF (r = 0.95, R = 0.92), group I ADC (r = 0.94, R = 0.99), and group II ADC (r = 0.93, R = 0.99). Adapted from reference [13]*

ISODATA technique enables automated clustering of "normal," "at risk" (perfusion–diffusion mismatch), and "ischemic core" tissues without any thresholds. Algorithms were developed to predict ischemic tissue fate on a pixel-by-pixel basis using acute phase CBF and apparent diffusion coefficient (ADC) data.[17-20]

Both ASL and DSC-MRI are widely used to image CBF in stroke. Tanaka *et al*. examined how changes in tissue spin–lattice relaxation time constant (T1), BBB permeability, and transit time affect CBF quantification by ASL and DSC in postischemic hyperperfusion in the same animals.[5] They found that in normal CBF pixels, ASL- and DSC-CBF linearly correlated pixel by pixel and in hyperperfusion pixels, ASL-CBF was significantly higher than DSC-CBF pixel by pixel (by 25%). In a normal animal injected with mannitol, which breaks BBB, CBF increases in the affected hemisphere. ASL yields a higher CBF increase than DSC [Figure 2]. They concluded that in normal tissue, ASL and DSC provide comparable quantitative CBF, whereas in postischemic hyperperfusion, ASL-CBF and DSC-CBF differ significantly because ischemia-induced changes in T1 and BBB permeability affect the two methods differently.

Postischemic hyperperfusion was also studied by Shen *et al*.[21] They found that late (>12 h) postischemic hyperperfusion was present consistently in the 30-min middle cerebral artery occlusion (MCAO) group, present in half of the animals in the 60-min MCAO group, and absent in the 90-min MCAO group. DSC, CBF, MRI, and maximum intensity projection (MRA) independently corroborated hyperperfusion detected by cASL; DSC and cASL showed essentially identical hyperperfusion territories at 48 h after occlusion [Figure 3a], although quantitative comparison was not performed. MRA at 48 h after occlusion of the same rat showed thicker and brighter blood vessels with many smaller branches becoming more apparent in the ipsilateral hemisphere compared with the contralateral hemisphere [Figure 3b]. MRA on day 7 showed that the ipsilateral arteries had similar size and brightness as the contralateral hemisphere (hyperperfusion had subsided) but they were tortuous.

Functional MRI based on CBF change is spatially more specific to the site of increased neural activity, is easier to interpret than the more commonly used blood-oxygenation-level-dependent (BOLD) fMRI signals, is less susceptible to pathological perturbations to the baseline signal, and has less intersubject and day-to-day variability. Figure 4 shows the CBF and BOLD fMRI responses to hypercapnic challenge in a stroke rat.[22] The hypercapnic challenge evoked a marked CBF increase in the normal left hemisphere, slightly attenuated CBF increase in the right hemisphere (RH) "normal" tissues, and essentially no evoked CBF increase in the RH ischemic "core" and "mismatch" tissues. Hypercapnia-induced CBF increases were essentially absent in regions with perfusion deficit. Interestingly, although dependent on the precise threshold used, the BOLD activated areas appeared to be larger than the CBF activation areas, suggesting differences in metabolic and CBF changes associated with ischemic injury. Shen *et al*. performed high spatial resolution CBF and BOLD fMRI measures to forepaw stimulation in rats.[23] The results showed that CBF fMRI responses peaked in layers IV–V, dropped in layers I–II and VI [Figure 5], whereas the BOLD fMRI responses peaked in the superficial layers II-III.

Unlike continuous ASL, which uses a flow-dependent inversion of arterial blood in the presence of a constant gradient and RF, pulsed ASL (PASL) uses a relatively short RF pulse to invert a slab of arterial blood. Pulsed ASL acquires flow-weighted images using a subtraction between flow-sensitive images using selective inversion and flow-insensitive images using

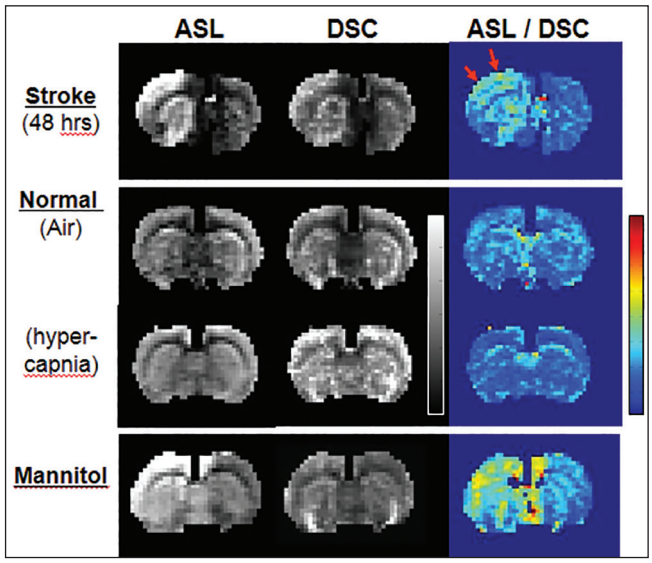

Figure 2: *Arterial spin labeling (ASL) cerebral blood flow (CBF) image, dynamic susceptibility contrast (DSC) CBF image, and ASL:DSC ratio maps from one animal of each of the three experimental groups. In the stroke animal (top row), the stroke lesion shows hyperperfusion. ASL yields a higher CBF than DSC. In the hypercapnia animal (middle row), CBF increases globally. ASL- and DSC-CBF maps show similar increases. In a normal animal injected with mannitol (bottom row), CBF increases in the affected hemisphere. ASL yields a higher CBF increase than DSC. Adapted from reference [5]*

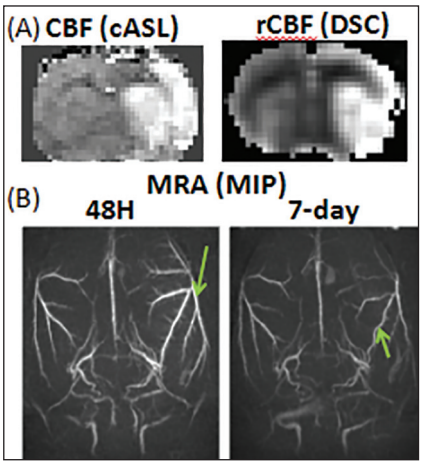

Figure 3: *(a) Cerebral blood flow (CBF) maps obtained by continuous arterial spin labeling (cASL) and DSC 48 h after occlusion from the same animal. Display CBF scale is 0-2 mL/g/min. DSC and cASL showed essentially identical hyperperfusion territories (b) Maximum intensity projection (MRA) at 48 h (thicker and brighter blood vessels with many smaller branches becoming more apparent in the ipsilateral hemisphere) and 7 days after occlusion (similar size and brightness in both hemispheres but tortuous in the ipsilateral hemisphere) from the same animal. Adapted from reference [21]*

nonselective inversion. Compared with CASL, pulsed ASL offers several advantages: less sensitivity to variations in T1 relaxation time, decreased inaccuracies in estimation of blood transit time, smaller influence of magnetization transfer, and markedly reduced specific absorption rate (SAR) exposure.[24] However, the overall signal is usually lower in PASL than in continuous ASL.[24] There were some but not many applications[25-29] of PASL in experimental stroke study.

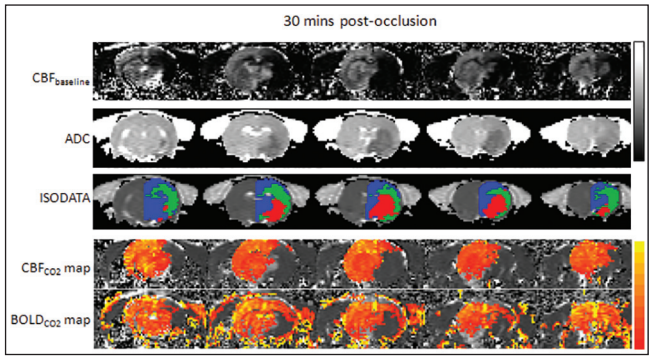

Figure 4: *Representative CBF and ADC maps, ISODATA clusters overlaid on ADC maps, ΔCBF_{CO2} and $\Delta BOLD_{CO2}$ percent change maps overlaid on CBF images of a rat subjected to permanent focal ischemia at the 30-min time point. ISODATA cluster analysis yielded "normal" (blue), "perfusion-diffusion mismatch" (green), and "ischemic core" (red) clusters. Hypercapnia-induced CBF increase was essentially absent in regions with perfusion deficit (core and mismatch). Interestingly, hypercapnia-induced BOLD response was still observable in the mismatch region. Grayscale bar indicates ADC 0-0.001 mm^2/s and CBF 0-3 mL/g/min. Color bar indicates ΔCBF 10-400% and ΔBOLD 1-10%. Adapted from reference [22]*

New Technical Developments of Cerebral Blood Flow Methods

Inversion-recovery background suppression continuous arterial spin labeling

In ASL MRI to measure CBF, pairwise subtraction of temporally adjacent nonlabeled and labeled images often cannot completely cancel the background static tissue signal because of temporally fluctuating physiological noise. While background suppression (BS) by inversion nulling improves CBF temporal stability, imperfect pulses compromise CBF contrast. Conventional BS techniques which apply the BS inversion pulses after the spin labelling and use the arterial transit time as the inversion delay, may not be applicable in small animals because the arterial transit time is short. Shen *et al*. presents an approach of BS to overcome these drawbacks using a separate "neck" radiofrequency coil for ASL and a "brain" radiofrequency coil for BS with the inversion pulse placed before spin labeling.[30] This approach is referred to as the inversion-recovery BS with the two-coil continuous ASL (IR-cASL) technique. The Bloch equations were modified to provide accurate CBF quantification at different levels of BS and for multislice acquisition where

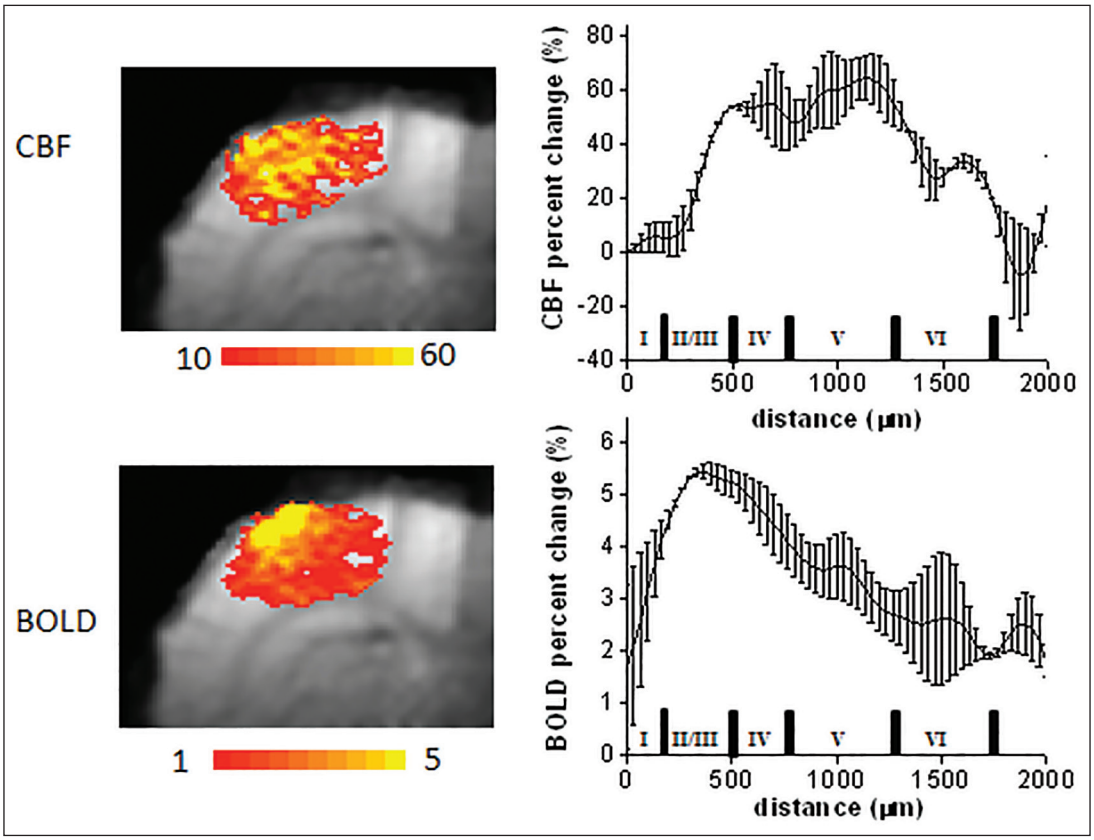

Figure 5: *The CBF and BOLD fMRI responses and spatial profiles at 100 × 76 × 1,000 μm^3 obtained using a smaller surface coil. CBF fMRI responses peaked in layers IV-V, dropped off in layers I-II and VI, whereas the BOLD fMRI responses peaked in the superficial layers II-III. The distance from 0 μm to 2,000 μm is from the cortical surface to corpus callosum boundary. Data were obtained from two animals with three repeated fMRI trials for each animal (mean ± SD). Adapted from reference [23]*

different slices have different degrees of BS and residual degree of labeling. Representative CBF maps of cASL and IR-cASL with labeling duration (LD) of 2 s are shown in Figure 6a. By visual inspection, cASL and IR-cASL showed similarly good CBF contrast. Whole-brain CBF values were similar across different labeling durations [Figure 6b]. To quantify the potential improvement, temporal standard deviation (SD) maps of normalized perfusion contrast were analyzed pixel by pixel [Figure 6c]. The whole-brain temporal SD for different LDs (from 1.4 s to 3.0 s) was plotted in Figure 6d. The whole-brain temporal SD of IR-cASL was significantly ($P < 0.05$) smaller than that of cASL for LD = 1.4-2.0 s because of the BS effect. At LD = 3.0 s, magnetization mostly recovered back to equilibrium and thus, IR-cASL and cASL yielded similar temporal SD as expected ($P = 0.09$). The temporal and spatial contrast-to-noise characteristics of basal CBF and CBF-based fMRI of hypercapnia stimulation in rats at 7 Tesla were also analyzed. IR-cASL yielded two times better temporal stability and 2.0-2.3 times higher functional contrast-to-noise ratios for hypercapnia stimulation compared with cASL without BS in the same animals. This technique has been applied in eye blood-flow images[31] where vitreous signals were suppressed to improve retinal and choroidal blood flow sensitivities.

High spatial resolution cerebral blood flow

The spatial resolution of MRI in animals is usually higher than that in human studies due to the smaller size of brains and therefore smaller coils and field of view. But it is still around 400~200 μm. High spatial resolution CBF MRI could provide important information on CBF supply to the brain at the columnar and laminar levels. Shen *et al*. implemented a high-resolution (up to 50 × 38 μm^2) CBF MRI protocol of the rat brain, created a digital CBF atlas, reported CBF values for 30+ brain structures based on the atlas, and explored applications of high-resolution CBF fMRI of forepaw stimulation.[23] Excellent blood-flow contrasts were observed among different cortical and subcortical structures [Figure 7]. CBF MRI showed column-like alternating bright and dark bands in the neocortices, reflecting the layout of descending arterioles and ascending venules, respectively [Figures 7 and 8]. CBF MRI also showed lamina-like alternating bright and dark layers across the cortical thicknesses, consistent with the underlying vascular density. CBF profiles across the cortical thickness showed two peaks in layers IV and VI and a shallow trough in layer V. Whole-brain CBF was about 0.89 mL/g/min, with the highest CBF values found among the neocortical structures (1 mL/g/min, range: 0.89-1.16 mL/g/min) and the lowest CBF values in the *corpus callosum* (0.32 mL/g/min), yielding a gray: white matter CBF ratio of 3.1. CBF fMRI responses peaked across layers IV–V, whereas the BOLD fMRI responses showed a peak in the superficial layers II-III. High-resolution basal CBF MRI, evoked CBF fMRI, and CBF brain atlas can be used to study neurological disorders (such as ischemic stroke). Figure 9 shows an example of the high-resolution (75 × 56 × 1000 μm^3) CBF images of a stroke rat before and after reperfusion. During MCAO, regions of normal perfusion and hypoperfusion were heterogeneous. Recannulation was successful and perfusion image showed heterogeneous blood flow with regions of hypoperfusion (i.e., thalamus) and hyperperfusion (i.e., S2).

Arterial spin labeling in mice

Continuous ASL MRI with a separate neck labeling coil provides a highly sensitive method to image CBF. In mice, however, this has not been possible because the proximity of the neck coil to the brain coil (~1 cm from center to center)

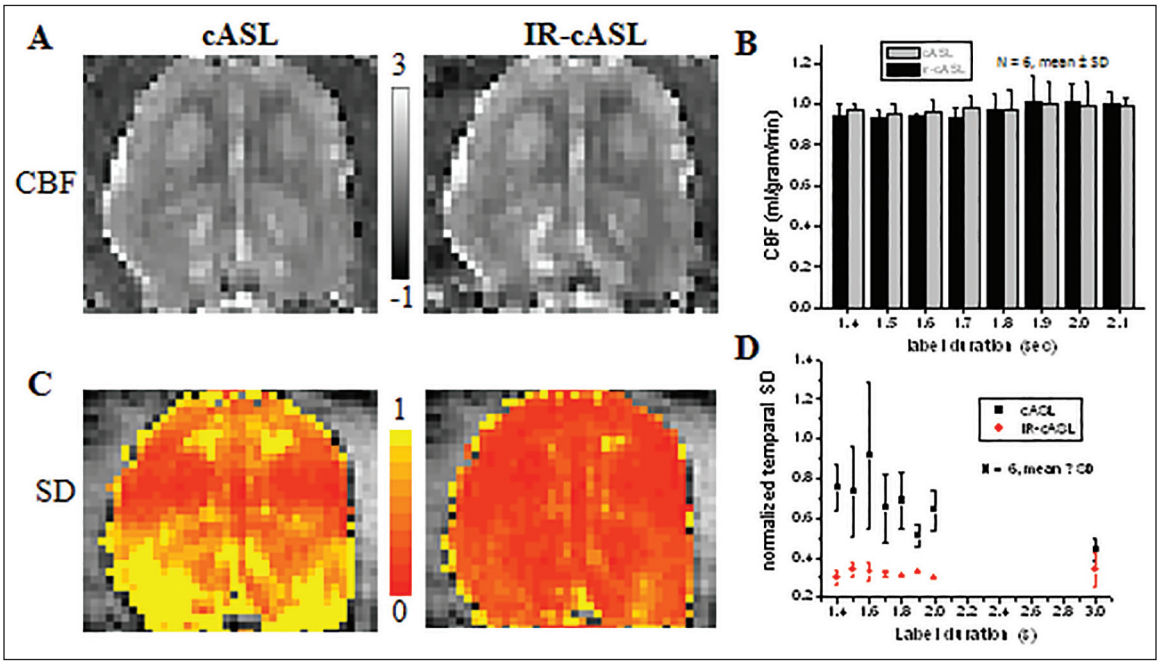

Figure 6: *(a) CBF images of cASL and IR-cASL acquisition (horizontal view) showed similarly good CBF contrast (b) CBF values versus labeling durations. Whole-brain CBF values were similar across different labeling durations. Scale bars indicate CBF units in mL/g/min (c) Temporal standard deviation maps of cASL and IR-cASL acquisition (LD = 2s) (d) Temporal standard deviations (SDs) of cASL and IR-cASL versus labeling durations. The whole-brain temporal SD of IR-cASL was significantly (P < 0.05) smaller than that of cASL for LD = 1.4-2.0 s because of the BS effect. At LD = 3.0 s, magnetization mostly recovered toward equilibrium and thus, IR-cASL and cASL yielded similar temporal SD as expected (P = 0.09). Adapted from reference [30]*

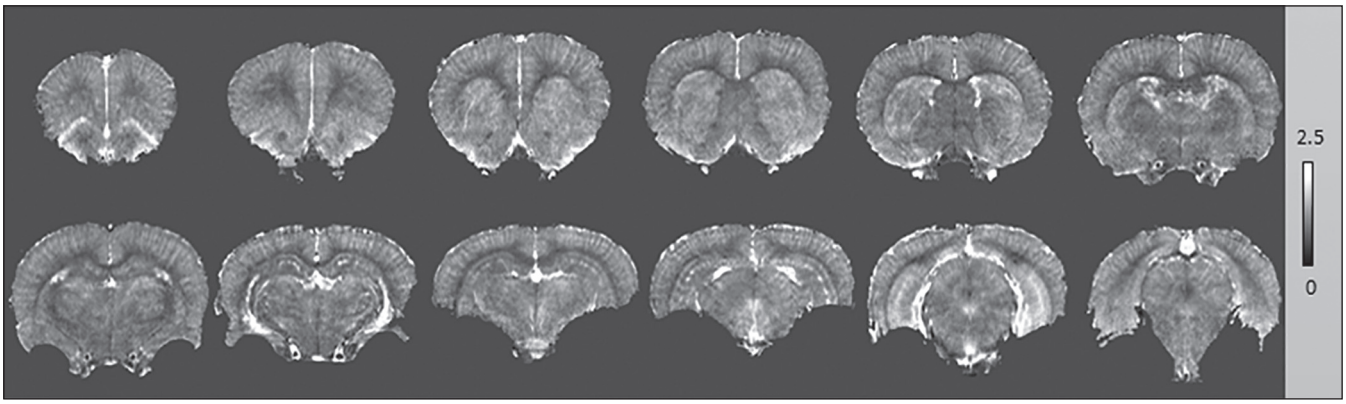

Figure 7: *Multislice high spatial resolution CBF images of a rat brain at 75 × 56 × 1,000 μm³ from one animal. Excellent blood-flow contrasts were observed among different cortical and subcortical structures. CBF MRI showed column-like alternating bright and dark bands in the neocortices, reflecting the layout of descending arterioles and ascending venules, respectively. Adapted from reference [23]*

results in significantly saturate of the brain signal by the neck coil. To overcome this limitation, the cardiac spin labeling (CSL) technique is introduced in which the labeling coil is placed at the heart's position.[32] To demonstrate its utility, CSL CBF was applied to image quantitative basal CBF and hypercapnia-induced CBF changes in mice. This approach provides a practical means to image CBF with high sensitivity in small animals, compares favorably to existing mouse CBF imaging techniques, and could broaden CBF applications in mice where many brain diseases and transgenic models are widely available. A small circular surface coil (ID = 1.1 cm) was placed on top of the head. A circular labeling coil (ID = 0.8 cm), built into the cradle, was placed at the heart's position for continuous CSL. The two coils were positioned parallel to each other, separated by 2 cm from center to center, and were actively decoupled. The heart label coil was a little bit off the center toward the left so that the mouse's heart could be right on top of the label coil. Figure 10 shows multislice CBF images of a representative mouse brain at 100 × 100 × 1000 μm³ resolution. This technique has been used to measure cerebral,[33] retinal, and choroidal[34-36] blood flow in mice.

Conclusions and Future Perspectives

This review summarized the theories and applications of the most commonly used perfusion measurement methods: DSC and ASL. DSC has the advantages of fast acquisition and can be readily implemented (no special sequence and hardware required). The disadvantage of DSC is that it requires an exogenous contrast agent, which precludes repeated measurements. By contrast, ASL is completely noninvasive, requiring no exogenous contrast agent or ionizing radiation. Repeated measurements can be made, which can be used for dynamic studies (i.e., fMRI), averaging to enhance SNR and/or spatial resolution.

Some new developments of CBF techniques in animal models were also summarized. Many techniques related to perfusion imaging were not included such as flow-sensitive alternating inversion recovery (FAIR),[37,38] modulation of tissue and vessel (MOTIVE),[39] vascular space occupancy (VASO),[40,41] and monocrystalline iron oxide nanocalloid (MION)-based CBV fMRI.[42,43] Many applications of CBF imaging, such as CBF imaging of traumatic brain injury (TBI)[44] and progressive hypertension,[45] were also not

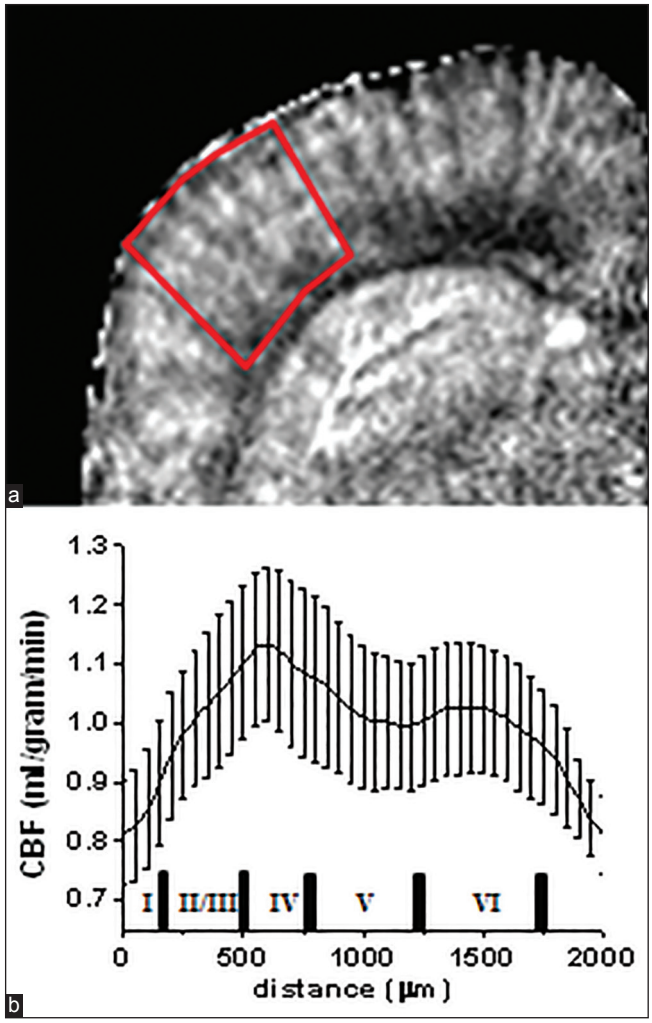

Figure 8: *Higher resolution CBF (a) images, and (b) profiles at 50 × 38 × 1,000 μm³ obtained using the smaller surface coil. In B, the distance from 0 μm to 2,000 μm is from cortical surface to corpus callosum boundary. Data were obtained from 4 animals (mean ± SD). CBF MRI showed lamina-like alternating bright and dark layers across the cortical thicknesses, consistent with the underlying vascular density. CBF profiles across the cortical thickness showed two peaks in layer IV and VI and a shallow trough in layer V. Adapted from reference [23]*

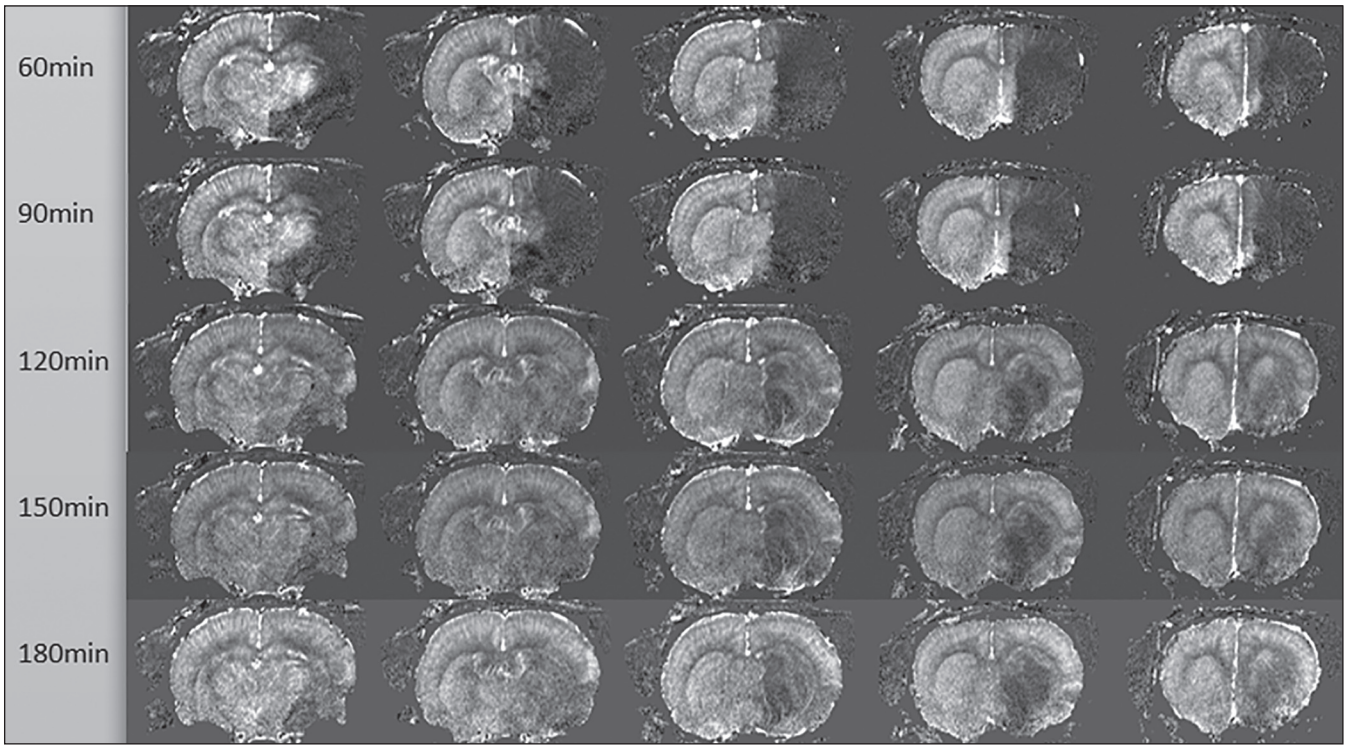

Figure 9: *High-resolution CBF maps of a MCAO stroke rat before and after reperfusion. The rat was reperfused after 90-min CBF acquisition. During MCAO, regions of normal perfusion and hypoperfusion were heterogeneous. Recannulation was successful and perfusion image showed heterogeneous blood flow with regions of hypoperfusion (i.e., thalamus) and hyperperfusion (i.e., S2) (Unpublished data)*

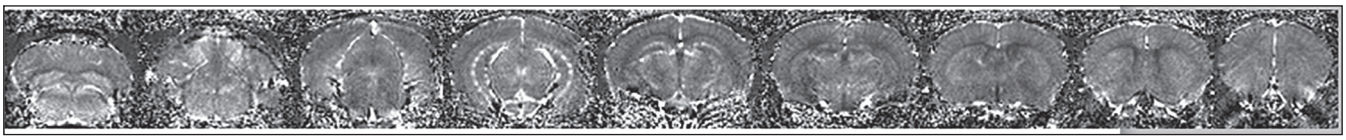

Figure 10: *Multislice mouse CBF images at 100 × 100 × 1,000 μm³. CBF images showed heterogeneous blood flow contrast, as expected. CBF is lower in the corpus callosum (white matter) compared to gray matter. Adapted from reference [32]*

included. Readers interested in those topics can read related publications.

Future development of CBF imaging will include high spatial and/or temporal resolution CBF, faster ASL-CBF acquisition, three-dimentional CBF achieved by the use of higher-field systems, compressed sensing, view sharing, and parallel imaging. Perfusion territory mapping would also be a very important and valuable asset to the diagnosis of a number of cerebrovascular diseases (please see a detailed review [46]).

Financial support and sponsorship
This work was supported by the NIH (R01-NS45879) and the American Heart Association (EIA 0940104N, SDG 0830293N and 12BGIA9300047).

Conflicts of interest
There are no conflicts of interest.

References

1. Jahng GH, Li KL, Ostergaard L, Calamante F. Perfusion magnetic resonance imaging: A comprehensive update on principles and techniques. Korean J Radiol 2014;15:554-77.
2. Rosen BR, Belliveau JW, Vevea JM, Brady TJ. Perfusion imaging with NMR contrast agents. Magn Reson Med 1990;14:249-65.
3. Edelman RR, Mattle HP, Atkinson DJ, Hill T, Finn JP, Mayman C, *et al*. Cerebral blood flow: Assessment with dynamic contrast-enhanced T2*-weighted MR imaging at 1.5 T. Radiology 1990;176:211-20.
4. Østergaard L. Principles of cerebral perfusion imaging by bolus tracking. J Magn Reson Imaging 2005;22:710-7.
5. Tanaka Y, Nagaoka T, Nair G, Ohno K, Duong TQ. Arterial spin labeling and dynamic susceptibility contrast CBF MRI in postischemic hyperperfusion, hypercapnia, and after mannitol injection. J Cereb Blood Flow Metab 2011;31:1403-11.
6. Bjornerud A, Sorensen AG, Mouridsen K, Emblem KE. T1- and T2*-dominant extravasation correction in DSC-MRI: Part I — Theoretical considerations and implications for assessment of tumor hemodynamic properties. J Cereb Blood Flow Metab 2011;31:2041-53.
7. Detre JA, Leigh JS, Williams DS, Koretsky AP. Perfusion imaging. Magn Reson Med 1992;23:37-45.
8. Gunther M, Oshio K, Feinberg DA. Single-shot 3D imaging techniques improve arterial spin labeling perfusion measurements. Magn Reson Med 2005;54:491-8.
9. Williams DS, Detre JA, Leigh JS, Koretsky AP. Magnetic resonance imaging of perfusion using spin inversion of arterial water. Proc Natl Acad Sci U S A 1992;89:212-6.

10. Kwong KK, Chesler DA, Weisskoff RM, Donahue KM, Davis TL, Ostergaard L, *et al*. MR perfusion studies with T1-weighted echo planar imaging. Magn Reson Med 1995;34:878-87.
11. Edelman RR, Siewert B, Darby DG, Thangaraj V, Nobre AC, Mesulam MM, *et al*. Qualitative mapping of cerebral blood flow and functional localization with echo-planar MR imaging and signal targeting with alternating radio frequency. Radiology 1994;192:513-20.
12. Wong EC, Cronin M, Wu WC, Inglis B, Frank LR, Liu TT. Velocity-selective arterial spin labeling. Magn Reson Med 2006;55:1334-41.
13. Shen Q, Meng X, Fisher M, Sotak CH, Duong TQ. Pixel-by-pixel spatiotemporal progression of focal ischemia derived using quantitative perfusion and diffusion imaging. J Cereb Blood Flow Metab 2003;23:1479-88.
14. Shen Q, Fisher M, Sotak CH, Duong TQ. Effects of reperfusion on ADC and CBF pixel-by-pixel dynamics in stroke: Characterizing tissue fates using quantitative diffusion and perfusion imaging. J Cereb Blood Flow Metab 2004;24:280-90.
15. Meng X, Fisher M, Shen Q, Sotak CH, Duong TQ. Characterizing the diffusion/perfusion mismatch in experimental focal cerebral ischemia. Ann Neurol 2004;55:207-12.
16. Shen Q, Ren H, Fisher M, Bouley J, Duong TQ. Dynamic tracking of acute ischemic tissue fates using improved unsupervised ISODATA analysis of high-resolution quantitative perfusion and diffusion data. J Cereb Blood Flow Metab 2004;24:887-97.
17. Shen Q, Ren H, Fisher M, Duong TQ. Statistical prediction of tissue fates in acute ischemic brain injury. J Cereb Blood Flow Metab 2005;25:1336-45.
18. Shen Q, Duong TQ. Quantitative prediction of ischemic stroke tissue fate. NMR Biomed 2008;21:839-48.
19. Huang S, Shen Q, Duong TQ. Artificial neural network prediction of ischemic tissue fate in acute stroke imaging. J Cereb Blood Flow Metab 2010;30:1661-70.
20. Huang S, Shen Q, Duong TQ. Quantitative prediction of acute ischemic tissue fate using support vector machine. Brain Res 2011;1405:77-84.
21. Shen Q, Du F, Huang S, Duong TQ. Spatiotemporal characteristics of postischemic hyperperfusion with respect to changes in T1, T2, diffusion, angiography, and blood-brain barrier permeability. J Cereb Blood Flow Metab 2011;31:2076-85.
22. Shen Q, Ren H, Cheng H, Fisher M, Duong TQ. Functional, perfusion and diffusion MRI of acute focal ischemic brain injury. J Cereb Blood Flow Metab 2005;25:1265-79.
23. Shen Q, Huang S, Duong TQ. Ultra-high spatial resolution basal and evoked cerebral blood flow MRI of the rat brain. Brain Res 2015;1599:126-36.
24. Wong EC, Buxton RB, Frank LR. A theoretical and experimental comparison of continuous and pulsed arterial spin labeling techniques for quantitative perfusion imaging. Magn Reson Med 1998;40:348-55.
25. Hofmeijer J, Schepers J, van der Worp HB, Kappelle LJ, Nicolay K. Comparison of perfusion MRI by flow-sensitive alternating inversion recovery and dynamic susceptibility contrast in rats with permanent middle cerebral artery occlusion. NMR Biomed 2005;18:390-4.
26. Hofmeijer J, Veldhuis WB, Schepers J, Nicolay K, Kappelle LJ, Bär PR, *et al*. The time course of ischemic damage and cerebral perfusion in a rat model of space-occupying cerebral infarction. Brain Res 2004;1013:74-82.
27. Leithner C, Gertz K, Schrock H, Priller J, Prass K, Steinbrink J, *et al*. A flow sensitive alternating inversion recovery (FAIR)-MRI protocol to measure hemispheric cerebral blood flow in a mouse stroke model. Exp Neurol 2008;210:118-27.
28. Thomas DL. Arterial spin labeling in small animals: Methods and applications to experimental cerebral ischemia. J Magn Reson Imaging 2005;22:741-4.
29. Wegener S, Artmann J, Luft AR, Buxton RB, Weller M, Wong EC. The time of maximum post-ischemic hyperperfusion indicates infarct growth following transient experimental ischemia. PLoS One 2013;8:e65322.
30. Shen Q, Duong TQ. Background suppression in arterial spin labeling MRI with a separate neck labeling coil. NMR Biomed 2011;24:1111-8.
31. Li G, Shih YY, Kiel JW, De La Garza BH, Du F, Duong TQ. MRI study of cerebral, retinal and choroidal blood flow responses to acute hypertension. Exp Eye Res 2013;112:118-24.
32. Muir ER, Shen Q, Duong TQ. Cerebral blood flow MRI in mice using the cardiac-spin-labeling technique. Magn Reson Med 2008;60:744-8.
33. Lin AL, Pulliam DA, Deepa SS, Halloran JJ, Hussong SA, Burbank RR, *et al*. Decreased *in vitro* mitochondrial function is associated with enhanced brain metabolism, blood flow, and memory in Surf1-deficient mice. J Cereb Blood Flow Metab 2013;33:1605-11.
34. Muir ER, De La Garza B, Duong TQ. Blood flow and anatomical MRI in a mouse model of retinitis pigmentosa. Magn Reson Med 2013;69:221-8.
35. Muir ER, De La Garza BH, Duong TQ. Retinal and choroidal blood flow in retinal degeneration. Magn Reson Med 2013;69:221-8.
36. Lavery W, Muir ER, Kiel JW, Duong TQ. Magnetic resonance imaging indicates decreased choroidal and retinal blood flow in the DBA/2J mouse model of glaucoma. Invest Ophthalmol Vis Sci 2012;53:560-4.
37. Kim SG, Tsekos NV. Perfusion imaging by a flow-sensitive alternating inversion recovery (FAIR) technique: Application to functional brain imaging. Magn Reson Med 1997;37:425-35.
38. Tsekos NV, Zhang F, Merkle H, Nagayama M, Iadecola C, Kim SG. Quantitative measurements of cerebral blood flow in rats using the FAIR technique: Correlation with previous iodoantipyrine autoradiographic studies. Magn Reson Med 1998;39:564-73.
39. Kim T, Kim SG. Quantification of cerebral arterial blood volume and cerebral blood flow using MRI with modulation of tissue and vessel (MOTIVE) signals. Magn Reson Med 2005;54:333-42.
40. Lu H, Golay X, Pekar JJ, Van Zijl PC. Functional magnetic resonance imaging based on changes in vascular space occupancy. Magn Reson Med 2003;50:263-74.
41. Lu H, Hua J, van Zijl PC. Noninvasive functional imaging of cerebral blood volume with vascular-space-occupancy (VASO) MRI. NMR Biomed 2013;26:932-48.
42. Mandeville JB, Marota JJ. Vascular filters of functional MRI: Spatial localization using BOLD and CBV contrast. Magn Reson Med 1999;42:591-8.
43. Shen Q, Ren H, Duong TQ. CBF, BOLD, CBV, and CMRO(2) fMRI signal temporal dynamics at 500-msec resolution. J Magn Reson Imaging 2008;27:599-606.
44. Long JA, Watts LT, Li W, Shen Q, Muir ER, Huang S, *et al*. The effects of perturbed cerebral blood flow and cerebrovascular reactivity on structural MRI and behavioral readouts in mild traumatic brain injury. J Cereb Blood Flow Metab 2015;35:1852-61.
45. Li Y, Shen Q, Huang S, Li W, Muir ER, Long JA, *et al*. Cerebral angiography, blood flow and vascular reactivity in progressive hypertension. Neuroimage 2015;111:329-37.
46. Paiva FF, Tannús A, Silva AC. Measurement of cerebral perfusion territories using arterial spin labelling. NMR Biomed 2007;20:633-42.